

Observation of Airy minimum in elastic and inelastic scattering of ^3He from ^{12}C at 50.5 and 60 MeV and alpha particle condensation in ^{12}C

Sh. Hamada¹, Y. Hirabayashi², N. Burtebayev³, and S. Ohkubo^{4,5}

¹*Faculty of Science, Tanta University, Tanta, Egypt*

²*Information Initiative Center, Hokkaido University, Sapporo 060-0811, Japan*

³*Institute of Nuclear Physics, Almaty, Kazakhstan*

⁴*Research Center for Nuclear Physics, Osaka University, Ibaraki, Osaka 567-0047, Japan and*

⁵*University of Kochi, 5-15 Eikokuji, Kochi 780-8515, Japan*

(Dated: June 14, 2021)

Angular distributions for elastic and inelastic scattering of ^3He from ^{12}C were measured at energies 50.5 and 60 MeV. The Airy minimum of the prerainbow scattering was clearly observed in the angular distributions for the 0_2^+ (7.65 MeV) state of ^{12}C (Hoyle state). The experimental results were analyzed with a coupled channels method with double folding potentials derived from the microscopic wave functions for the ground 0_1^+ , 2^+ (4.44 MeV), 3^- (9.64 MeV) and 0_2^+ states. The analysis supports the view that the Hoyle state is a three alpha particle condensate with a large radius of dilute matter distribution.

PACS numbers: 25.55.Ci, 27.20.+n, 21.60.Gx, 03.75.Nt

I. INTRODUCTION

The well observed α -cluster structure of excited states of ^{12}C has been a subject of significant interest [1]. Especially, much attention has been paid to the α -cluster structure of the 0_2^+ state at $E_x=7.65$ MeV (Hoyle state), which is 0.38 MeV above the 3α threshold. As early as 1954, Hoyle showed [2] that this level plays an extremely important role in nucleosynthesis. The properties of the Hoyle state in ^{12}C determine the ratio of carbon to oxygen formed in the stellar helium burning process that strongly affects the future evolution of stars. Our complete knowledge about the unique structure of this state is far from complete [3]. This state has a developed 3α cluster structure with an enlarged radius, which has been confirmed by theoretical cluster models such as the 3α generator coordinate method [4] and the 3α resonating group method [5].

The 3α structure of ^{12}C was most thoroughly investigated by Uegaki *et al.* in their pioneering work [4], which showed that the Hoyle state has a dilute structure in a new “ α -boson gas phase” and clarified the systematic existence of a “new phase” of the 3α particles above the α threshold. Tohsaki *et al.* [6] suggested a condensate structure for the 0_2^+ state, where the 3α -clusters are condensed into the lowest s-state of their potential. Bose-Einstein condensation (BEC) has been well established in a dilute gas of cold atom clusters [7]. Much effort has been devoted to understanding the alpha particle condensation of the Hoyle state of ^{12}C [8–20]. If the Hoyle state is a dilute state due to BEC of 3α particles, then it should be possible to observe physical properties characteristic to it such as a huge radius. To measure such radius of the excited state is very challenging.

The purpose of this paper is to report the measurement of the angular distributions of ^3He scattering from ^{12}C at 50.5 and 60 MeV and to observe the Airy minimum for elastic and inelastic scattering including the excitation

to the Hoyle state. The shift of the Airy minimum for the Hoyle state toward larger angles compared with the ground state is found in the coupled channel analysis of the experimental data using a double folding model. This supports alpha particle condensation of the Hoyle state.

The paper is organized as follows. In Sec. II the experimental procedure is given and in Sec. III the method used for the theoretical analysis of the experimental data is presented. Section IV is devoted to the results of the experimental data, its theoretical analysis and discussion. The summary is given in Sec. V.

II. EXPERIMENTAL PROCEDURE

The experimental measurements of angular distributions in elastic and inelastic scattering of ^3He from ^{12}C at incident energy $E_L=50.5$ and 60 MeV were performed at the isochronous cyclotron U-150M INP NNC located in Almaty-Kazakhstan, which allows accelerating protons up to energy 30 MeV, deuterons up to energy 25 MeV, ^3He up to energy 60 MeV and α -particles up to energy 50 MeV. Charged particles produced in the cyclotron at the source, which is located in the central part of the chamber in an arc discharge, by applying an appropriate gas (hydrogen, deuterium, helium 3 and helium 4). Their acceleration takes place in the interpolar space of a 1.5 meter magnet at the time of flight of particles between the dees. The energy spread of the beam was determined by measuring the energy spectrum of particles elastically scattered by a thin target of gold located in the scattering chamber. In this case, measurements at small angles (10°) can be used to avoid errors due to inaccurate knowledge of the target thickness and angular spread of particles in the beam. For absolute energy scale calibration, three alpha sources ($^{241,243}\text{Am}+^{244}\text{Cm}$) were used.

The ^3He ion beam was accelerated up to energies 50.5

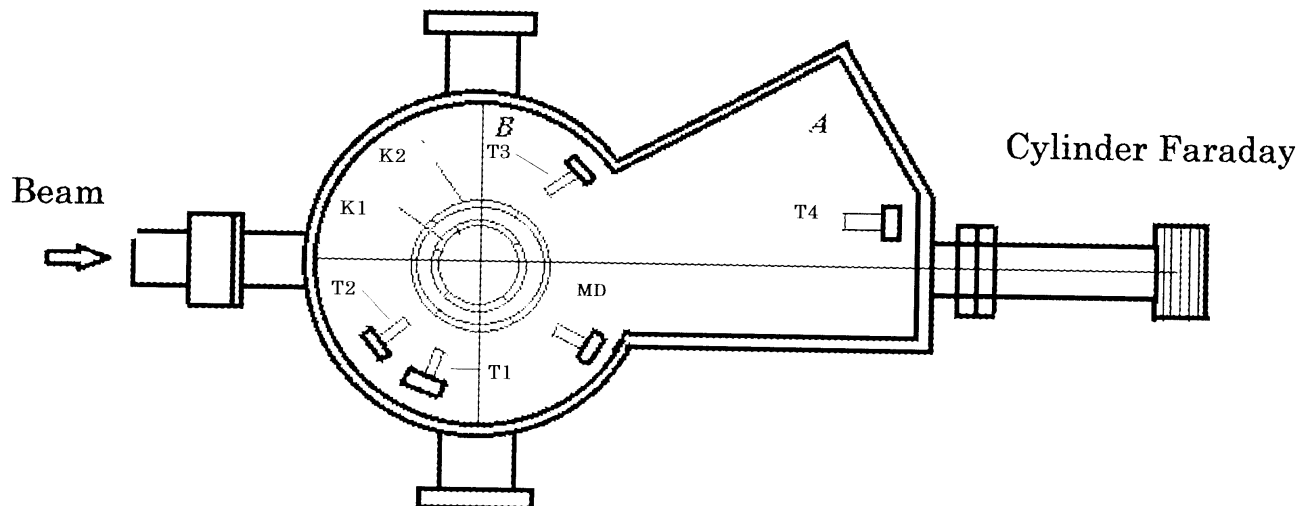


FIG. 1: The layout of the scattering chamber used for the experiment.

and 60 MeV and then directed to a ^{12}C target of thickness $30\mu\text{g}/\text{cm}^2$. The experiments were conducted in the scattering chamber shown in Fig. 1. The stainless steel scattering chamber made consists of a hollow cylinder with an internal diameter 715 mm, height 370 mm, and the so-called “pocket” A, which is an additional volume, elongated along the beam. In the bulk B of the chamber, there are three (ΔE - E) telescopes of silicon semiconductor detectors, which cover the scattering angles of 10 - 70° . A fourth telescope with independent drive, designed for covering the measurements in the angular range of 2 - 20° , resides in volume A. The considerable distance from the target to the detectors (1000 mm) allows the load on the detecting apparatus due to the elastic scattering measurements at extremely small angles to be reduced by a factor of 10-15. A monitoring window with a diameter of 290 mm located on the top cover of the chamber allows visual inspection of the experimental situation (angles of the telescopes, the state of the target, etc.). For optimal focusing of the accelerated ^3He ions on the target, two collimators of diameter 2 mm were used. The pumping system, which includes a high-vacuum turbo molecular pump and pre-evacuation, was tested and achieved high vacuum inside the chamber of about 2.3×10^{-6} Pa.

The (E - ΔE) method was used in the registration and identification of reaction products. The method is based on simultaneous measurement of specific energy losses of charged particles in matter (dE/dx) and the total kinetic energy E . The method is based on the Bethe-Bloch theory, connecting the energy of charged particles emitted from their specific ionization in matter:

$$\frac{dE}{dx} = \frac{kMz^2}{E} \quad (1)$$

where the constant k is weakly dependent on the type of particle, M and z are mass and charge of emitted parti-

TABLE I: The volume integral per nucleon pair J_V , root mean square radius $\langle R^2 \rangle^{1/2}$, of the real folding potential, and the parameters of the imaginary potentials in the conventional notation in elastic and inelastic scattering of ^3He from ^{12}C at $E_L = 50.5$ and 60 MeV. The normalization factor N_R is fixed to 1.28.

E_L (MeV)	J^π	J_V (MeV fm ³)	$\langle R^2 \rangle^{1/2}$ (fm)	W (MeV)	R_W (fm)	a_W (fm)
50.5	0_1^+	431	3.58	6.0	5.5	0.4
	2^+	427	3.56	11.0	5.0	0.2
	3^-	489	3.83	13.0	5.1	0.2
	0_2^+	565	4.38	16.0	5.8	0.9
60	0_1^+	420	3.58	7.0	5.0	0.4
	2^+	415	3.56	6.0	5.0	0.2
	3^-	476	3.83	13.0	5.1	0.2
	0_2^+	548	4.38	12.0	5.5	0.9

cles. This relationship shows that each type of particle is represented by a hyperbola in the coordinate space ($E, \Delta E$). Thus through the simultaneous measurement of E and dE/dx , the desired type of particle can be selected. In the telescope detectors “ E - ΔE ”, ΔE - detector is a surface-barrier silicon detectors firm ORTEC- thick active layer of 30 to 200 μm with thin inlet ($\sim 40\mu\text{g}/\text{cm}^2$ Au) and outlet ($\sim 40\mu\text{g}/\text{cm}^2$ Al) windows. The complete absorption E detector is used as a stop detector. It is manufactured by ORTEC and uses high-purity silicon of thickness 2 mm.

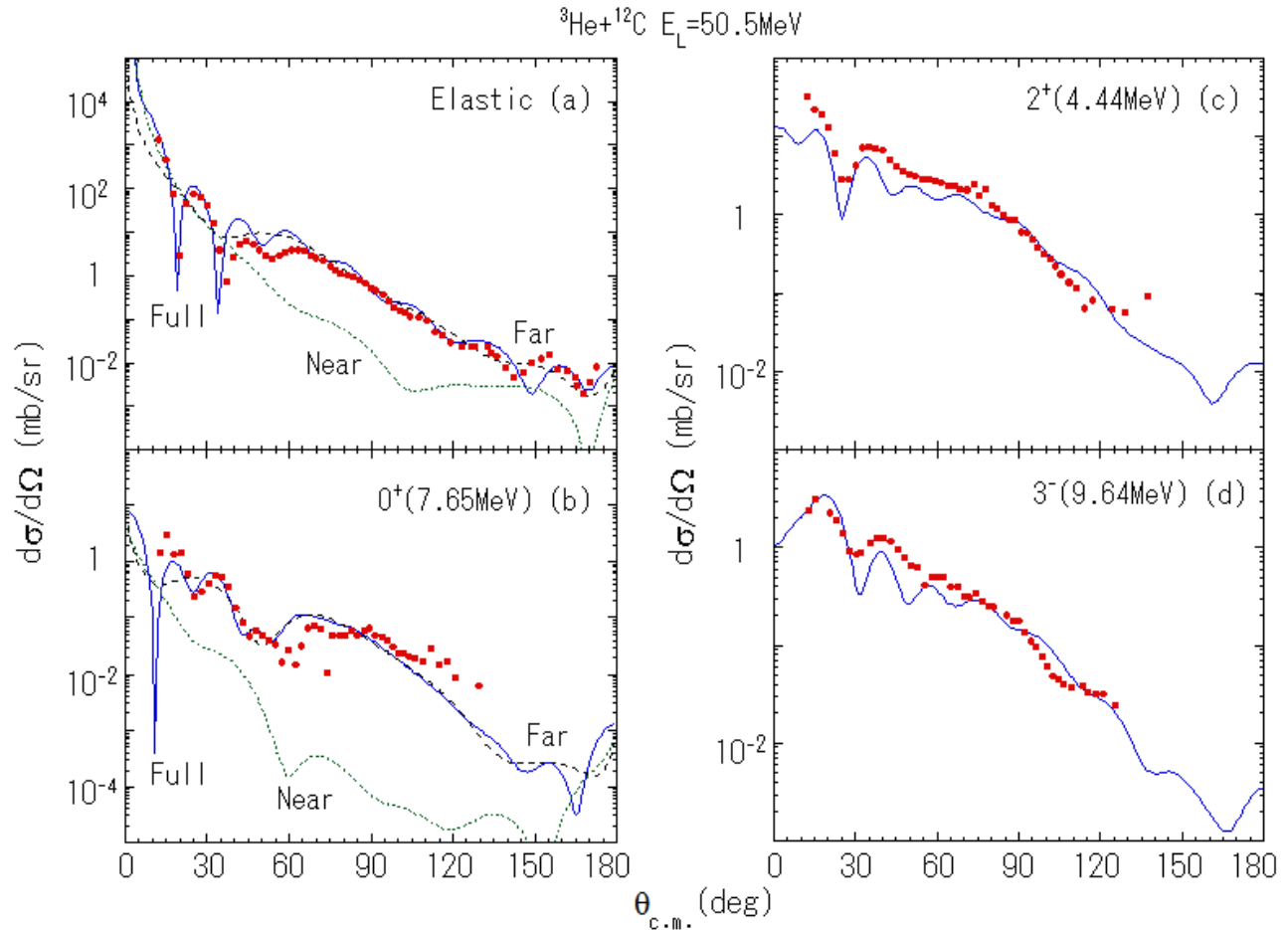


FIG. 2: (Color online) Comparison between the experimental (points) and the calculated differential cross sections for elastic and inelastic scattering of ${}^3\text{He}$ from ${}^{12}\text{C}$ at $E_L = 50.5$ MeV: (a) ground state (0.0 MeV), (b) 2^+ (4.44 MeV), (c) 0_2^+ (7.65 MeV) and (d) 3^- (9.64 MeV) using coupled channel method. The calculated cross sections (solid lines) are shown decomposed into the farside component (dashed lines) and the nearside component (dotted lines).

III. METHOD OF THEORETICAL ANALYSIS

We study elastic and inelastic ${}^3\text{He}+{}^{12}\text{C}$ scattering using the microscopic coupled channel method by simultaneously taking into account the 0_1^+ (0.0 MeV), 2^+ (4.44 MeV), 0_2^+ (7.65 MeV), and 3^- (9.64 MeV) states of ${}^{12}\text{C}$. The diagonal and coupling potentials for the ${}^3\text{He}+{}^{12}\text{C}$ system are calculated by the double folding model:

$$V_{ij}(\mathbf{R}) = \int \rho_{00}^{(3\text{He})}(\mathbf{r}_1) \rho_{ij}^{(12\text{C})}(\mathbf{r}_2) \times v_{\text{NN}}(E, \rho, \mathbf{r}_1 + \mathbf{R} - \mathbf{r}_2) d\mathbf{r}_1 d\mathbf{r}_2, \quad (2)$$

where $\rho_{00}^{(3\text{He})}(\mathbf{r})$ is the ground state density of ${}^3\text{He}$ taken from Ref.[21], while v_{NN} denotes the density-dependent M3Y effective interaction (DDM3Y) [22]. $\rho_{ij}^{(12\text{C})}(\mathbf{r})$ represents the diagonal ($i = j$) or transition ($i \neq j$) nucleon density of ${}^{12}\text{C}$ calculated in the resonating group method by Kamimura [23]. This coupled-channel method was successfully used in the analyses of the elastic and inelas-

tic scattering of ${}^3\text{He}$ from ${}^{12}\text{C}$ at $E_L = 34.7$ and 72.0 MeV [24]. In the calculation of densities of ${}^{12}\text{C}$, the shell-like structure of the ground state 0_1^+ , 2^+ , and 3^- states, and the well-developed α -cluster structure of the 0_2^+ state are both well reproduced. These wave functions have been checked against many experimental data including charge form factors and electric transition probabilities involving excitation to the 0_2^+ state [23]. In the analysis we introduce the normalization factor N_R for the real part of the potentials and phenomenological imaginary potentials with a Woods-Saxon form factor for each channel (Table I). The normalization factor N_R is fixed to 1.28, the same as was used for a previous analysis of ${}^3\text{He}+{}^{12}\text{C}$ [24].

IV. RESULT AND DISCUSSION

In Fig. 2, angular distributions calculated using the potentials from Table I are shown in comparison with

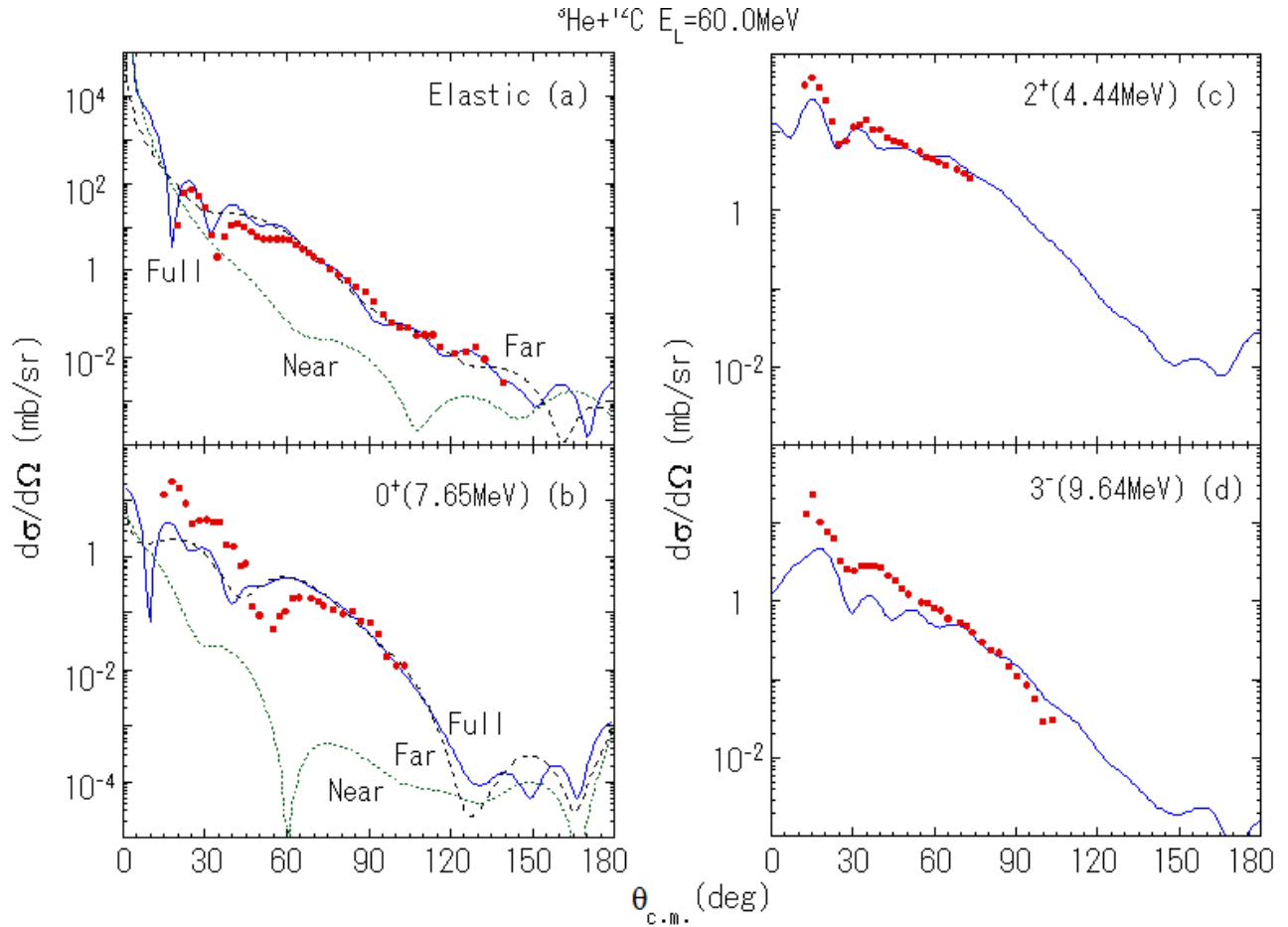


FIG. 3: (Color online) Same as Fig. 2 but for $E_L=60$ MeV.

the experimental data for elastic and inelastic scattering of ${}^3\text{He}$ ions beam from a ${}^{12}\text{C}$ target at energy $E_L=50.5$ MeV. The calculated cross sections are decomposed into the farside and nearside components. In the intermediate and large angular regions the scattering is dominated by the farside component, which shows that the scattering in this energy region is refractive. The Airy minimum can be observed for elastic scattering and inelastic scattering to the Hoyle state. The characteristic features of the falloff of the cross sections beyond the rainbow angle [9] in the experimental angular distributions for the shell-like ground, 2^+ , 3^- states, and the 0_2^+ state with the well-developed α -cluster structure are simultaneously well reproduced. It is noted that for the ground and the 2^+ states the agreement of the calculations with the data is fairly good up to large angles. Fig. 3 shows the comparison between the experimental data and the theoretical calculations at energy $E_L=60$ MeV. The discrepancy between the experimental data and the calculations is seen for the 0_2^+ state in Fig. 2(b) and Fig. 3(b). One of the causes might be due to the truncation of the explicit coupling to the higher excited states. For example, most of the imaginary potentials for the 0_2^+ state come from the coupling to the 2_2^+ state, which has a well-developed α -

cluster structure with almost the same configuration as the 0_2^+ state.

To identify the position of the Airy minimum observed in the experimental angular distributions clearly, in Fig. 4 the theoretical angular distribution for $E_L=50.5$ MeV calculated by switching off the imaginary potential in the coupled channel method is decomposed into the farside and nearside components. As the scattering is caused by the real potential only, the features of refractive scattering such as Airy minima can be seen without being obscured by absorption. In Fig. 4(a), we see that the minimum at 35° in the calculated angular distribution for elastic scattering comes from the farside component. Thus the minimum at this angle in the calculated angular distribution is assigned as the first order Airy minimum $A1$ caused by refractive scattering. Although the minimum in the experimental data of elastic scattering is obscured by the effect of the imaginary potential and the nearside component, we can identify uniquely the position of the Airy minimum in the experimental data. As for the inelastic scattering to the Hoyle state, in Fig. 4(b) a clear minimum is seen in the calculated angular distribution at 55° and the minimum is fully due to the farside component of the angular distribution because

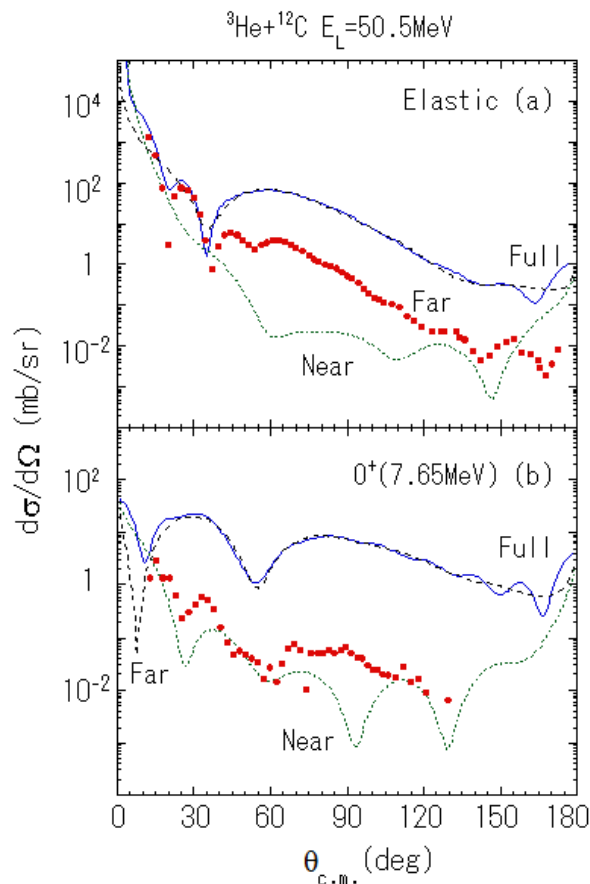


FIG. 4: (Color online) Differential cross sections of ^3He scattering from ^{12}C at $E_L = 50.5$ MeV calculated using coupled channel method by switching off the imaginary potential ($W=0$); (a) elastic and (b) inelastic scattering to the 0_2^+ (7.65 MeV). The calculated cross sections (solid lines) are shown decomposed into the farside component (dashed lines) and the nearside component (dotted lines) and compared with the experimental data (points).

the contribution of the nearside component is negligible. We can identify this minimum as the first order Airy minimum $A1$ due to refractive scattering to the Hoyle state. The Airy minimum $A1$ at the intermediate angular region where the farside scattering dominates is scarcely obscured by the presence of the imaginary potential. Therefore we can identify the $A1$ Airy minimum for inelastic scattering to the Hoyle state without ambiguity. We note in Fig. 4(b) that the second order Airy minimum appears at forward angle around 10° in the calculated angular distribution for inelastic scattering to the Hoyle state. This shows that the refraction in inelastic scattering to the Hoyle state is much stronger than that in elastic scattering. In the experimental data the second Airy minimum is washed out by the effect of absorption and diffractive scattering dominates in the very forward angular region. We have checked that the same situation appears for the $E_L=60$ MeV case.

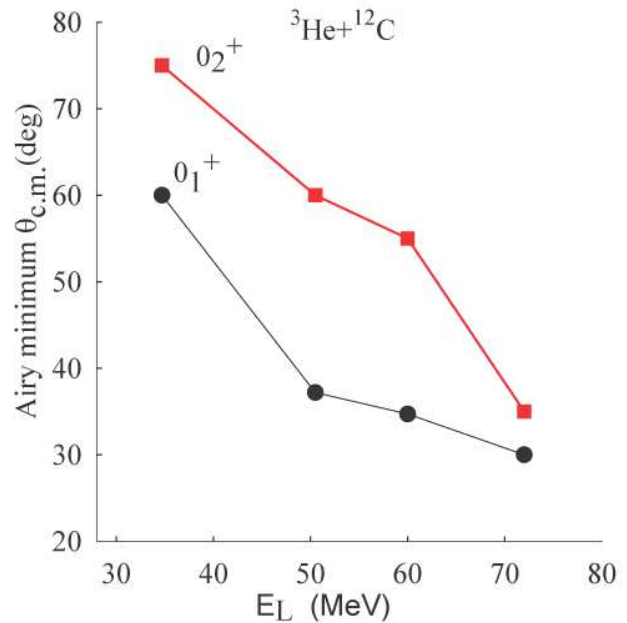


FIG. 5: (Color online) Angular position of the Airy minimum $A1$ for the 0_1^+ and 0_2^+ (7.65 MeV) states of ^{12}C in $^3\text{He} + ^{12}\text{C}$ scattering versus the incident energy. The data at $E_L=34.7$ MeV and 72 MeV are from Ref.[24]. The lines are only to guide the eye.

In Fig. 2, the first Airy minimum $A1$ at $E_L=50.5$ MeV due to refractive scattering is identified at 37° for elastic scattering and $\sim 60^\circ$ for the 0_2^+ state. In Fig. 2(b), the experimental angular distribution to the Hoyle state shows two small valleys in the intermediate angular region with a minimum at 58° and 62° , respectively. It seems that these two valleys are fragmented from the broad valley structure of the Airy minimum (as seen in the theoretical curve in Fig.4(b)) located at around 60° . Therefore it seems reasonable to consider that the centroid 60° is a minimum due to refractive scattering, i.e., the Airy minimum rather than the individual small two minima at 58° and 62° . In Fig. 3 at $E_L = 60$ MeV, the first Airy minimum $A1$ is identified at 35° for elastic scattering and 55° for the 0_2^+ state. In Fig. 5 the position of the Airy minimum for the ground and the 0_2^+ state of ^{12}C in $^3\text{He} + ^{12}\text{C}$ scattering at different energies (50.5, 60, 34.7 and 72 MeV) are summarized. It is clearly shown that the $A1$ minimum for the 0_2^+ state is shifted to a larger angle. A more precise prerainbow Airy oscillation is seen in inelastic scattering to the Hoyle state than in elastic scattering. The refractive effect of the 0_2^+ state is more clearly seen in the prerainbow structure at a low incident energy region than at a high incident energy region where a typical nuclear rainbow appears. This shows that the refractive effect is significantly stronger for the 0_2^+ state than the ground state.

In Table I we see that the r.m.s. radius of the potential, which is a lens for refractive scattering, for the 0_2^+ state

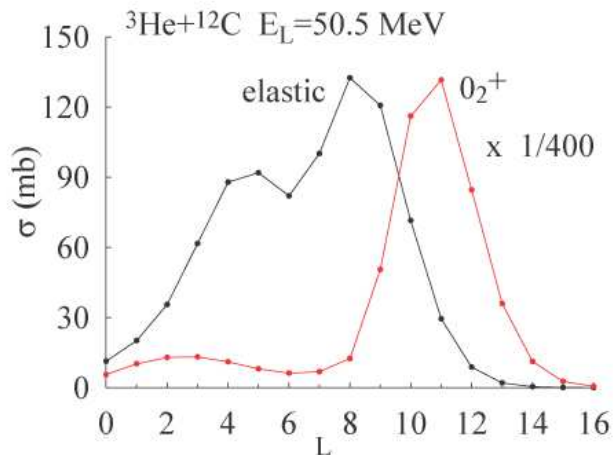


FIG. 6: (Color online) Calculated partial cross sections for elastic ${}^3\text{He}+{}^{12}\text{C}$ scattering and inelastic scattering to the 0_2^+ (7.65 MeV) state at $E_L=50.5$ MeV are shown as a function of the orbital angular momentum L between ${}^3\text{He}$ and ${}^{12}\text{C}$.

is much more extended than that for the ground state in agreement with the dilute distribution of the density of the 0_2^+ state. In Fig. 6 calculated partial cross sections scattered to the ground state and the 0_2^+ state are displayed. We see that the inelastic scattering to the Hoyle state occurs at very large angular momenta (large ra-

dius) compared with the elastic scattering. These facts account for the shift of the Airy minimum of the Hoyle state to a larger angle and support the idea that the Hoyle state has a large radius compared with the normal ground state. These results are consistent with those obtained from refractive scattering of α particle scattering from ${}^{12}\text{C}$ [9, 24–26].

V. SUMMARY

We have measured the angular distributions of elastic and inelastic scattering to the 2^+ (4.44 MeV), 0_2^+ (7.65 MeV) and 3^- (9.64 MeV) states of ${}^{12}\text{C}$ by bombarding ${}^3\text{He}$ ions on the thick target at energies 50.5 and 60 MeV at the isochronous cyclotron U-150M INP NNC. The experimental angular distributions were analyzed in the coupled channel method using a double folding model in which the realistic wave functions for ${}^{12}\text{C}$ calculated in the microscopic cluster model were used. It is found that the position of the Airy minimum in the angular distribution for the 0_2^+ state is clearly shifted toward large angles in comparison with that of ground state, which indicates that the root mean square radius for the state is larger than that of the ground state. This finding supports the idea that the 0_2^+ (7.65 MeV) state of ${}^{12}\text{C}$ has a dilute density and an enlarged radius due to the condensation of 3α clusters.

-
- [1] M. Freer, Rep. Prog. Phys. **70**, 2149 (2007).
[2] F. Hoyle, Astrophys. J. Suppl. **1**, 121 (1954).
[3] M. Freer, *Physics of Unstable Nuclei, Proceedings of the International Symposium on Phys. of Unstable Nuclei IS-PUN07*, edited by D. T. Khoa *et al.* (World Scientific, Singapore, 2008), p. 10.
[4] E. Uegaki, S. Okabe, Y. Abe, and H. Tanaka, Prog. Theor. Phys. **57**, 1262 (1977).
[5] Y. Fukushima and M. Kamimura, *Proceedings of the International Conference on Nuclear Structure, Tokyo, 1977*, edited by T. Marumori (J. Phys. Soc. Japan Suppl. **44**, 225 (1978)).
[6] A. Tohsaki, H. Horiuchi, P. Schuck, and G. Röpke, Phys. Rev. Lett. **87**, 192501 (2001).
[7] A. J. Leggett, Rev. Mod. Phys. **73**, 307 (2001).
[8] Y. Funaki, A. Tohsaki, H. Horiuchi, P. Schuck, and G. Röpke, Phys. Rev. C **67**, 051306(R) (2003).
[9] S. Ohkubo and Y. Hirabayashi, Phys. Rev. C **70**, 041602(R) (2004).
[10] M. Chernykh, H. Feldmeier, T. Neff, P. von Neumann-Cosel, and A. Richter, Phys. Rev. Lett. **98**, 032501 (2007).
[11] A. N. Danilov, T. L. Belyaeva, A. S. Demyanova, S. A. Goncharov, and A. A. Ogloblin, Phys. Rev. C **80**, 054603 (2009).
[12] Ad. R. Raduta *et al.*, Phys. Lett. **B705**, 65 (2011).
[13] M. Freer *et al.*, Phys. Rev. C **83**, 034314 (2011).
[14] W. R. Zimmerman, N. E. Destefano, M. Freer, M. Gai, and F. D. Smit, Phys. Rev. C **84**, 027304 (2011).
[15] M. Itoh *et al.*, Phys. Rev. C **84**, 054308 (2011).
[16] J. Manfredi *et al.*, Phys. Rev. C **85**, 037603 (2012).
[17] M. Freer *et al.*, Phys. Rev. C **86**, 034320 (2012).
[18] C. Kurokawa and K. Katō, Phys. Rev. C **71**, 021301 (2005); Nucl. Phys. **A738**, 455c (2004).
[19] Y. Kanada-En'yo, Prog. Theor. Phys. **117**, 655 (2007).
[20] C. Kurokawa and K. Katō, Nucl. Phys. **A792**, 87 (2007).
[21] J. Cook and R. J. Griffiths, Nucl. Phys. **A366**, 27 (1981).
[22] A. M. Kobos, B. A. Brown, R. Lindsay, and G. R. Satchler, Nucl. Phys. **A425**, 205 (1984).
[23] M. Kamimura, Nucl. Phys. **A351**, 456 (1981).
[24] S. Ohkubo and Y. Hirabayashi, Phys. Rev. C **75**, 044609 (2007).
[25] S. Ohkubo and Y. Hirabayashi, AIP Conference Proceedings No. **1012**, Frontiers in Nuclear Structure, Astrophysics, and Reactions, FINUSTAR2, 2007, eds. P. Demetriou, R. Julin, and S. V. Harissopoulos (American Institute of Physics), p.407-409.
[26] S. Ohkubo and H. Hirabayashi, Journal of Physics Conference Series **111**, 012014 (2008).